Coupling otolith microstructure analysis and hydrographic backtracking suggests a mechanism for the 2000s North Sea herring recruitment failure

Ross, Stine Dalmann; Payne, Mark; Worsøe Clausen, Lotte; Nash, Richard D.M.

Publication date:
2012

Document Version
Publisher's PDF, also known as Version of record

Not to be cited without prior reference to the author ICES CM 2012/J:14

Coupling Otolith Microstructure Analysis and Hydrographic Backtracking Suggests a Mechanism for the 2000s North Sea Herring Recruitment Failure

Stine D. Ross*, Mark R. Payne, Lotte Worsøe Clausen, Peter Munk, Henrik Mosegaard and Richard D.M. Nash

Abstract

The North Sea autumn spawning herring (*Clupea harengus* L.) has, since the 2002 year class, shown an unprecedented sequence of ten years of sharply reduced recruitment, in spite of a high spawning biomass and low fishing mortality. Recent work has identified this reduction in recruitment level (or stock productivity) as taking place during the larval over-wintering phase: however, the underlying mechanism remains elusive. In this study we analysed archived larval samples captured both before and after the onset of the reduced survival to test the hypothesis of a reduction in the larval growth rate. Individual larval growth rates, averaged over the 30 days prior to capture, were estimated for two hundred larval otoliths from four different years using a model-based analysis of the ring widths. The otolith measurements were complemented with additional information derived from hydrographic backtracking models (*e.g.* average temperature experienced, time available for feeding and spawning origin) to reconstruct the recent history of the larvae. A mixed-modelling approach was then employed to analyse the combined data: after correcting for the effect of the other variables, a significant reduction in larval growth rate, associated with the onset of the reduced recruitment, was identified. These results suggest that the reduced recruitment is associated with a reduction in the growth rate of the larval survivors, most probably through changes in either the amount or quality of the available food. Furthermore, this study demonstrates how coupling two different techniques (otolith microstructure analysis and hydrographic modelling) can yield unique insights into fish ecology.

Keywords: North Sea herring; larvae; otolith microstructure; hydrographic backtracking; growth; recruitment

Stine D. Ross* National Institute of Aquatic Resources (DTU-Aqua), Technical University of Denmark, 2920 Charlottenlund, Denmark, +45 35883341. sdro@aqua.dtu.dk

Mark R. Payne National Institute of Aquatic Resources (DTU-Aqua), Technical University of Denmark, 2920 Charlottenlund, Denmark. & Environmental Physics, Institute of Biogeochemistry and Pollutant Dynamics, ETH Zürich, Universitätsstrasse 16, 8092 Zürich, Switzerland. mpa@aqua.dtu.dk

Lotte Worsøe Clausen National Institute of Aquatic Resources (DTU-Aqua), Technical University of Denmark, 2920 Charlottenlund, Denmark. law@aqua.dtu.dk

Peter Munk National Institute of Aquatic Resources (DTU-Aqua), Technical University of Denmark, 2920 Charlottenlund, Denmark. pm@aqua.dtu.dk

Henrik Mosegaard National Institute of Aquatic Resources (DTU-Aqua), Technical University of Denmark, 2920 Charlottenlund, Denmark. hm@aqua.dtu.dk

Richard D. M. Nash Institute of Marine Research, PB 1870 Nordnes, 5817 Bergen, Norway. richard.nash@imr.no

Introduction

In recent years the North Sea autumn spawning herring (*Clupea harengus* L.) stock has shown a markedly reduced production of juvenile fish (recruitment) (Payne et al., 2008). Starting from the 2002 year class, the stock has produced ten successive weak year classes (2002-2011) (ICES, 2012). This reduced recruitment has occurred regardless of an adult population (spawning stock biomass) at a size well above a level where it may impair recruitment concurrently with a fishing mortality that is well below, the levels where it can be expected to impact the production of juveniles (ICES, 2012). The recruitment of the stock has shown changes of shorter duration (Payne et al., 2008), but the robustness and enduring stability of this reduced stock productivity suggests that fundamental changes have taken place in the processes controlling the productivity.

The reduced productivity appears to be a consequence of reduced survival during the relatively long larval period (from spawning in autumn until metamorphosis in late-winter/early-spring) (Payne et al., 2008; see also Figure 1). This has occurred previously, albeit over a much shorter time *e.g.* the 1988-1990 year classes (Nash and Dickey-Collas, 2005). The increased larval mortality has also been traced further back into the early life-history through analysis of field-based observations, and is thought to occur closer to spawning than to metamorphosis (Fässler et al., 2011).

In spite of the insight into the dynamics of this stock and its long history of scientific investigations (Cushing and Bridger, 1966; Sinclair, 2009; Dickey-Collas et al., 2010) a full mechanistic understanding of the recruitment remains elusive. Many hypotheses have been proposed, however there is, as yet, no clear consensus. Temperature increases in the North Sea have been widely reported and shown to be associated with increased larval mortality (Payne et al., 2008; Fässler et al., 2011). Bioenergetics models have suggested that the time around yolk-sack absorption and first-feeding may represent a critical juncture for survival, again possibly related to temperature (Hufnagl and Peck, 2011). Changes in the zooplankton community in the North Sea are also known to have occurred (Edwards et al., 2007) and may have changed the quality or suitability of food available for North Sea herring. Parasite indicators have also suggested changes in the feeding patterns (S. Lusseau unpublished data).

A recurring theme amongst all of these hypotheses are processes affecting the growth rate of the larvae, either directly or indirectly. For example, changes in the zooplankton community could give rise to changes in either the quantity or quality of available food, and thereby alter the growth rate. Alternatively, changes in water temperature (assuming no changes in food) can alter the energy utilisation of the individuals leading again to changes in growth rate. Changes in growth-rate can then influence changes in survival, either indirectly via size/growth-specific predation, or directly through starvation mortality (Leggett and DeBlois, 1994; Houde, 2002).

Growth, as suggested elsewhere (Anderson, 1988), represents a “rational theoretical framework” for approaching this problem. Therefore, we examine whether the reduction in larval survival rate of North Sea autumn spawning herring from before to after 2001 is associated with a reduction in the growth rate during the larval phase.

Measuring growth rates in the field is typically challenging, and virtually impossible in a retrospective manner. However, the analysis of otolith microstructure in archival collections of larvae is a powerful tool for determining life history trajectories such as somatic growth. The otolith microstructure is strongly influenced by the environmental conditions, such as temperature (Folkvord et al., 2004) and food availability (Johannessen et al., 2000), experienced during the larval phase. Where feeding conditions are sufficient for growth herring larvae can deposit daily increments on their otoliths and thus the appearance of the individual larval otolith microstructure can be used as a proxy for the general growth conditions (Geffen, 1982; McGurk, 1984; Folkvord et al., 2000; Pavlov et al., 2000; Fox et al., 2004).

Hydrographic backtracking offers an alternative source of information about the environment experienced by ichthyoplankton (Batchelder, 2006; Christensen et al., 2007; Thygesen, 2011). Modern oceanographic circulation models provide estimates of the local currents and oceanographic properties at relatively high temporal and spatial resolutions. By releasing simulated “larvae” into these modelled fields and following them in an individual-based lagrangian manner, it is possible to produce a set of trajectories that describe the advection of these particles and the conditions they experience along the way. Furthermore, by running time backwards from a given end point (*e.g.* the position and time where a larvae was captured), it is possible to infer both where the larvae originated and the environmental history before capture.

In the present work we combine these two techniques, otolith microstructure analysis and hydrographic backtracking. We analyse the otoliths microstructure of archived larvae from a North Sea sampling program (reference to MIK series) to infer the growth rates obtained close to the point at which they were captured. We compliment these findings with results from the backtracking analyses to “add-value” to the observations in a manner that is not otherwise readily available. Finally, we apply mixed-effects modelling to combine these two data sources into a single analysis that allows us to test the hypothesis of reduced growth-rates being associated with a reduction in recruitment to the stock.

Materials and Methods

Survey data and Sample Archive

Late-stage herring larvae have been surveyed in the North Sea on a consistent basis since 1977, first by the International Young Herring Survey (IYHS) and since 1984 by the International Bottom Trawl Survey (IBTS). The survey takes place between January and March each year and is performed in a synoptic manner by a multinational fleet of research vessels and covers the entire North Sea region. The gear used was initially an Isaacs-Kidd Midwater trawl (Isaacs and Kidd, 1953), but the standard gear was changed in 1991 to a 2 metre ring net, generally referred to as an MIK (ICES, 2006). The sampling program is used to generate an index of larval abundance known as the IBTS-0 index (ICES, 2012). Ethanol preserved larvae were available from 1995 to the present from the Danish sampling sectors of the IBTS.

Otolith analysis and profile generation

Hauls selected for analysis were obtained from the Danish larval archive to ensure broad spatial coverage across the region sampled by *RV Dana* and to cover two years prior to (1998,1999) and after (2003, 2004) the onset of the 2000s reduction in per-capita recruitment.

Larvae from a given haul were rinsed and measured to the nearest millimetre (rounded down). Individual larvae were then selected to ensure a full and even coverage of the length distribution within the haul. The sagittal otoliths were extracted under a dissecting microscope and mounted in thermoplastic resin (Buehler Thermoplastic Cement no. 40–8100) at 140^{o}C to facilitate grinding and polishing The mounted otoliths were viewed and photographed using a LeicaTM DMLB compound light microscope (transmitted light) with long working-distance objective lenses (20x to 126x magnification) to facilitate viewing the otolith microstructure through a microscope slide 1.5 mm thick. If necessary, the otoliths were polished using a series of grinding and polishing films (3M^{TM}) with decreasing grain sizes from 10 µm to 0.3 µm to optimise the visual resolution at one focal plane. Digital images were analysed using ImagePro^{TM} 5.0 image-analysis package for WindowsTM.

An overview picture (20x magnification) was first used to obtain measurements of the length and width (major and minor axes) of the otolith. Otoliths that were chipped, cracked, broken or where it was not possible to obtain reliable measurements of both axes were discarded from the analysis. A high-magnification picture (80-126x magnification) was taken of the edge region of the otolith in the direction where both the otolith radius was at its largest and the rings most easily resolved. Images were then converted to grey-scale for analysis.

Profiles of increment widths as a function of radial distance were derived from these pictures. Increment widths were, in the first instance, measured automatically using the “Caliper” tool in

ImagePro using a profile bandwidth of 10 μm with a "falling point of inflection" detection criteria. The process was monitored by an expert reader, and if the program produced obviously erroneous increments (*e.g.* because of cracks in the otolith), these were altered manually to fit the visually-determined increments. In cases where the increments were not sufficiently clear to be identified by the Caliper tool or by eye, or where there were no detectable ring structures, no increment widths were reported and the region was flagged for exclusion in further analyses. Furthermore, a minimum acceptable increment width was set at 0.5 μm, to filter out the segments where false or no daily rings were visible along the measurement axis. A second reader then performed a quality check on these measurements to remove as much subjectivity as possible. The widths and radial position (measured from the edge of the otolith to the centre of the ring) were recorded for each validated ring and used as the basis for further analysis. The analysis procedure was repeated for at least two nearly-parallel but distinct radii for each otolith to provide both redundancy in the increment width profiles and increase the precision of estimation. Finally, the radial distance from the edge of the otolith to the centre along each of the profiles was determined from the 20x magnification picture.

Otolith profile analysis

Previous studies of larval herring growth have typically used a otolith ring-counting approach and hence size-at-age for growth estimation, *(e.g* Munk et al., 1991; Brophy and King, 2007). However, here we use a ring-width based approach as a way to circumvent some of the potential problems associated with accurate ageing of herring larvae and allowing for an estimation of the associated uncertainty when measuring the daily increments.

The analysis is predicated on the assumption that the relative deposition rate of material on the otolith is independent of the direction. The shape of the otolith is therefore maintained during the growth process, with regions with large radii growing proportionally faster (in absolute terms) than those with smaller radii. Otolith ring width is given as:

$$\frac{w_{i\theta}}{R_\theta} = \omega_{i\theta} = \omega_i \qquad (1)$$

where $w_{i\theta}$ is the absolute width of ring i in some arbitrary direction θ, R_θ is the radius of the otolith in the same direction and $\omega_{i\theta}$ is the relative width of the i-th ring. $\omega_{i\theta}$ is assumed to be independent of the angular direction and therefore we can simply write ω_i in place of $\omega_{i\theta}$. Under this assumption, relative changes in the ring-widths measured along different radial profiles can be compared directly.

We expect, however, that the noise in the individual ring-width measurements will be relatively large, due to the inherent difficulty of making these measures. We therefore apply a spline-smoother to this data to generate an estimate of the underlying mean ring-width, and to integrate measurements from separate profiles:

$$\omega_i = s\left(\frac{w_{i\theta}}{R_\theta}\right) + p_\theta + \epsilon_i \quad (2)$$

where

$$\sum_j p_j = 0 \quad (3)$$

where *s()* is a spline-smoother and p_θ is a constant offset factor for the profile taken in direction θ. Furthermore, we assume that errors in the residuals are normally distributed with a mean of zero and variance of σ^2, but also allow for correlation between residuals within the same profile *i.e.*

$$\epsilon_i \sim N(0, \sigma^2) \quad (4)$$

$$cor(\epsilon_{s\theta}, \epsilon_{t\theta}) = 1 - exp(-d_{st}/R_\theta \tau) \quad (5)$$

where $\varepsilon_{s\theta}$ and $\varepsilon_{t\theta}$ are residuals within the same profile θ, d_{st} is the absolute distance between rings *s* and *t*, and τ is a parameter characterising the relative distance over which the correlation occurs.

This system of equations represents a flexible approach to analysing the ring widths profiles, and allows for both systematic deviations in the growth rate (through the p_θ factor) and dependency structures in the results, where appropriate. However, in cases where these corrections are not required, the p_θ and τ parameters become zero and the model will collapse to a simple smoother with independent residuals *i.e.*

$$\omega_i = s\left(\frac{w_{i\theta}}{R_\theta}\right) + \epsilon_i \quad (6)$$

$$\epsilon_i \sim N(0, \sigma^2) \quad (7)$$

Once the smoothed ring-width profiles have been obtained, a mean-growth rate can be determined by first solving for the relative distance from the edge, ρ_n, at which the desired number of rings, *n*, are to be found *i.e.*

$$n = \int_0^{\rho_n} \frac{1}{s(r)} dr \quad (8)$$

where *r* is a dummy variable and *s()* is the smoother function fitted previously in equation 2. Equation 8 can be understood as integrating the inverse of the smoothed ring widths (*i.e.* the ring density) with respect to the relative radial distance, to estimate the total number of rings over the interval [0, ρ_n] .

Finally, the mean absolute otolith growth rate, *g*, (in μm per ring) can be calculated as follows:

$$g = \frac{\rho_n R_m}{n} \quad (9)$$

where R_m is the mean radius of the otolith (*i.e.* mean of the major and minor axes).

All smoothing calculations were performed using the "`mgcv`" package in R (Wood, 2006).

Uncertainty estimates for the smoothed estimate of the mean ring width, *s()*, were generated as part of the smoothing procedure and propagated through the calculations in the standard manner. Following the recommendations of (Wood, 2006), a spline "gamma" parameter of 1.4 was utilised to avoid overfitting of the data.

Hydrographic backtracking

The otolith-microstructure-derived larval-growth estimates were complemented with additional data derived through the use of hydrographic-back-tracking techniques. The theory underpinning this technique has been detailed elsewhere (Batchelder, 2006; Christensen et al., 2007; Thygesen, 2011). Briefly, a set of particles representing larvae are "released" in an oceanographic circulation model at an appropriate point in time and space. The particles are treated as lagrangian tracers and transported according to the local (modelled) currents and turbulence. When running in a back-tracking mode, time is run backwards and therefore the trajectories generated are indicative of the source of the particles, rather than their destination.

A back-tracking analysis was performed for each haul from which larval otoliths were analysed. The particle-tracking was performed using the Individual Based Modelling library (IBMlib) (Christensen et al. 2012, In Prep) forced with offline hourly physical fields from the Norwegian Ecological Model System (NORWECOM) for the North Sea (Skogen et al., 1995; Skogen and Søiland, 1998; Aksnes et al., n.d.). For each haul, 10 000 particles were released and tracked backwards in time from the date and position of capture until the previous 1 July: water temperature experienced by the larvae, photoperiod and the spatial position were stored at daily intervals. Particles were treated as purely passive tracers, with the exception that they had to remain in the upper 60m of the water column, consistent with observations (Heath et al., 1988). As the particle trajectories were therefore independent of larval size, it was sufficient to generate a single set of trajectories for each haul, and apply the same trajectory for each larvae used from that haul.

Trajectories were analysed and used to assign a most-likely spawning location to the larvae observed in a given haul. This was a necessity since assuming there is natal fidelity of herring to their spawning grounds (McQuinn, 1997) there could be inherent differences in the growth characteristics for each of the components or sub-stocks. Therefore, the extent of different sources of larvae needed to be determined. Five potential spawning regions and times were defined based on larval surveys of the spawning grounds (*i.e.* the International Herring Larval Survey, IHLS (Heath, 1993) (Table 1)). For a given haul and point in time, the proportion of particles in each of the spatial spawning regions was calculated and these proportions then averaged over the duration of the corresponding spawning period. The resulting value was then interpreted as a proxy of how many of the larvae observed in the haul originated from each potential spawning ground: each individual haul was then assigned a most-likely-spawning origin based on this approach.

Furthermore, the simulated particles also integrated fields thought to be of relevance to the growth of herring larvae. For each particle, the integrated temperature (degree-days), together with the integrated photoperiod (number of daylight hours, a proxy for feeding potential) was stored as a function of time. For a given haul, mean temperature and photoperiod over a given time span could then be calculated and incorporated into further analyses.

Data Analyses

The central hypothesis of this work was tested using linear mixed-effects modelling. Estimates of otolith-growth were matched with variables derived from the hydrographic-backtracking to provide a detailed description of the individual larval and the environment that it recently experienced. The modelling procedure followed a standard backward-selection approach, starting from a "beyond-optimal" model (*sensu* (Zuur et al., 2009)), incorporating all fixed and random effects. The beyond-optimal model used was multiplicative in nature *i.e.*

$$\log(g_i) = \beta_1 l_i + \beta_2 T_i + \beta_3 pp_i + \beta_4 yr_i + \beta_5 comp_i + b_j + \epsilon_i \quad (10)$$

$$b_j \sim N(0, \sigma^2_{haul})$$

$$\epsilon_i \sim N(0, e_i^2 \sigma^2_{resid})$$

where g_i is the mean otolith growth rate *i*, l_i is the length of larvae i, T_i is the mean temperature experienced by larvae *i* during the period leading up to capture, pp_i is the mean photoperiod during this time, yr_i is the year in which the larvae was captured, and $comp_i$ is the spawning component where it originated. b_j is a random effect for haul *j* (*i.e.* the haul that larvae *i* was captured in), assumed to be distributed normally with a mean of zero and variance σ_{haul}^2. ε_i is the residual, assumed to be normally distributed with a mean of zero and variance $e_i^2 \sigma_{resid}^2$, where e_i is the relative uncertainty in the estimated growth rate (g_i) and σ_{resid}^2 is a parameter to scale this variance accordingly.

The random effects elements of the model were tested using Likelihood ratio tests based on models fitted by restricted maximum likelihood (REML) (Zuur et al., 2009). Refinement of the fixed-effects component was performed using both marginal *F*-tests (based on REML fits) (Pinheiro and Bates, 2000) and Likelihood-ratio tests (based on Maximum Likelihood (ML) fits) (Zuur et al., 2009) in parallel. The final model fit was assessed using standard model diagnostic tools.

All mixed-effects models were fitted using the "`nlme`" package (Pinheiro and Bates, 2000) in R.

Results

Larvae were processed following the procedures detailed above, however, a number of larval otoliths were cracked or damaged as a result of the processing, or it was not otherwise possible to obtain reliable ring-width profiles. These samples (approximately 10% of selected larvae) were excluded from the analysis. The spatial coverage in the North Sea of the samples was constrained by the spatial coverage of the larval collection. The hauls were chosen to maximise the spatial coverage thus the samples covered a broad part of the central North Sea (Figure 2a). Larval samples covered two consecutive years prior to the onset of the recruitment failure (1998, 1999) and two consecutive years after the onset (2003, 2004) (Figure 2b). Larvae were selected from within a haul to cover the range of length classes present. The usable larvae samples ranged between 20 and 40mm in length, with the majority lying between 25 and 35mm and the median being 30mm (Figure 2c). In total, usable ring-width profiles were obtained for 197 larvae and used for further processing.

Larval-otolith morphology showed a strong relationship with the length of the larvae. The size of the otoliths (defined here as the mean of the major and minor radii) was significantly and positively correlated with the length of the larvae (Figure 3a; slope = 14.7±1.0 μm/mm, R^2= 0.81, *t*-test for positive slope: $p<0.001$). Changes in otolith size therefore appear to be an appropriate proxy for changes in the length of the larvae in this size range.

Otolith shape also changes with increasing larval length (Figure 3b). The eccentricity of the otolith (defined as the ratio of the major axis to minor axis) was minor (typically less than 10% difference in the axes) in the smallest larvae. However, a change in the slope is clearly visible around 25-30mm, beyond which the larval otoliths start to elongate appreciably: fitting a break-point regression model, where the eccentricity is constant below the breakpoint and increases above, suggests that this change occurs between 26 and 27mm. In general, the development of otolith shape is indeed an ontogenetic process reaching beyond the earliest life stages that can reshape the overall otolith outline, regardless of individuals and small-scale environmental conditions (Vignon, 2012).

Changes in the shape of the otolith may affect the relationship between the size of the otolith and the size of the larvae. However, visual inspection (*e.g.* from Figure 3a) does not suggest that this is a major effect. Fitting a quadratic rather than linear model to this relationship suggests an improvement in fit: however, the change is barely significant (Likelihood ratio test: LR = 4.014, df = 1, p=0.045) and is driven by a single outlier point with a high leverage. We therefore conclude that deviations from linearity are minor, and that there is therefore little support for a change in the assumption of a linear otolith-size-larval-length relationship.

The otolith ring-width approach employed here appears to be capable of handling noisy and missing ring-width measurements. Most of the otolith photographs exhibited regions where it was not possibly to clearly define rings due to irregularities in the ring formation process, the presence of dust, air bubbles and other contaminants on the mounted sample or variations in the focal plane (*e.g.* Figure 4). However, the use of multiple ring-width profiles along nearly parallel-axes added an alternative source of information in the obscured regions that could be utilised by spline-smoother applied here (Figure 5a). The spline smoother also handled regions around the otolith edge, where it is frequently not possible to measure rings. The smoother extrapolates into this region, based on trends in regions where there are data, but also increases the uncertainty associated with the extrapolated ring widths appropriately (Figure 5a).

The structure of the smoothing model also allowed sufficient flexibility to model more complex processes in the data (*e.g.* autocorrelation in the residuals, systematic differences in ring-widths between profiles: equation 2). In around 45% of cases, the Aikaike Information Criteria (AIC) (Zuur et al., 2009) suggested that these extra terms were not-needed, with a simple spline-smoother (equation 6) representing the data adequately. The full model (equation 2) was nevertheless employed in all cases for reasons of consistency. All fits were checked visually using standard modelling diagnostics (quantile-quantile plots, residual distribution plots, auto-correlation functions): in all cases the smoothing of the ring-width profiles in this manner appeared appropriate.

Smoothed ring-width profiles were then used to generate estimates of otolith-growth rates. Integrating the ring-density (*i.e.* the inverse ring-width: equation 9) as a function of distance from the edge yielded a profile (with associated uncertainties) of the number of rings against distance from the edge. It was found that nearly all otolith-edge pictures contained sufficient information to estimate the amount of otolith-growth in the 21 rings before the edge. The integrated-ring-number versus distance profiles for each otolith (together with the otolith mean-size) were then used to estimate the otolith growth in the 21 rings leading up to the edge (i.e. prior to capture) (Figure 5b).

Hydrographic backtracking models were used to generate additional information about the history of the larvae. Particles seeded at the point in model time and space where each larvae was captured were tracked backward in time (Figure 6a) to identify a distribution of potential trajectories that could lead to the point of capture. By comparing the distribution of the particles in time and space with the known spatial and temporal spawning domain of each component (Figure 6b), it was therefore possible to identify the spawning component where the larvae originated. Furthermore, environmental data such as the mean temperature (Figure 6c) and the mean photoperiod (*i.e.* number of hours per day of daylight, which is a proxy for the time available for visual-feeding: Figure 6d) were also generated and added to the analysis as additional sources of information.

The backtracking results gave insight into the larvae analysed. The majority of the larvae (80%) sampled in this study were from the central Banks and Buchan spawning components, with just 10% coming from each of the Downs and Orkney-Shetland components (Figure 7a). No west-of-Scotland larvae were identified amongst the sampled larvae. Mean temperatures prior to capture differed between larvae by up to three degrees (Figure 7b). Furthermore, systematic differences in temperature were found between the individual years (linear model: *temp ~ year* likelihood ratio test for deletion of year factor $p < 0.001$). Differences in mean photoperiod of up to 1.5 hours were also observed (Figure 7c): these differences were mainly found between the individual components (linear model: *light ~ component*, likelihood ratio tests for deletion of component term $p = 0.002$). These data suggest that there are systematic environmental differences between the larvae that may need to be accounted for in later stages of the analysis.

Preliminary data exploratoration examined the data collected with a view to undertaking linear modelling and followed the protocol suggested by (Zuur et al., 2010). Five covariates were considered as explanatory variables (larvae length, year of collection, mean photoperiod, mean temperature, and spawning component) together with the estimated growth rate and its associated uncertainty. No major outliers were identified in the continuous variables. A small number of (unusually large) outliers were apparent in the growth-rate uncertainties: however, as these were to be used as weighting factors in the later analysis, the corresponding samples were retained because the large uncertainties would effectively down-weight them out of the analysis anyway. Potential collinearity was examined by calculating variance inflation factors (VIFs) between the explanatory variables. The largest of these (for the spawning component variable) was 2.6, less than the thresholds of 10 (Montgomery et al., 2001) and 3 (Zuur et al., 2007) suggested elsewhere: no adjustments for collinearity were therefore employed. Potential interactions between variables were considered and examined using coplots (Zuur et al., 2010) but there was no visual evidence to support their presence. Furthermore, the data available is highly unbalanced (*c.f.* Figure 7a), and for some interactions sparse or lacking: it was therefore decided not to consider interactions in the analysis.

The otolith-growth data was analysed using a linear mixed-effects model (Pinheiro and Bates, 2000; Zuur et al., 2009). The initial “beyond optimal” model used log-growth rate as the dependent variable, all five covariates (without interactions) as explanatory variables (fixed effects), the haul identifier as a random effect and the relative uncertainties in the growth-rates as weighting factors (equation 10). The random-effects component was tested against a simpler model with no random-effect term and found to be significant (Likelihood ratio test, corrected for testing on the boundary: LR = 8.60, df=1, p=0.002). Model diagnostics of the “beyond-optimal” model suggested that it showed a good fit to the data and that the underlying assumptions were appropriate. Refinement of the fixed-effects component lead to the dropping of the photoperiod and component terms: the final model therefore retained length, temperature

and year as significant fixed effects (Table 1). Model diagnostics of this final model also showed an excellent fit to the data: the residuals appeared to be independent of the fitted growth rate (Figure 8a), the larvae length (Figure 8b), the mean temperature (Figure 8c), and the photoperiod, year and spawning component (not shown) and appeared homoscedastic (variance constant) in all cases. Furthermore, both the residuals (Figure 8d) and the random-effects (not shown) appeared normally distributed. The model therefore appears to fit the data well.

The coefficients of the mixed effects model (Table 1) give insight into the factors affecting the larval growth-rates. The growth-rate is seen to be higher the larger the larvae and the lower the mean temperature, both of which effects are significant at the 1% level. The year effect is also significant (marginal *F*-test based on a REML fit: F=4.64, df= 3,40, p=0.007), suggesting a significant inter-annual variability even after the other factors have been accounted for.

The combined contributions of the temperature and year effects suggest that the year effect is stronger than the temperature effect. As noted above, there are significant differences between the years in terms of the temperatures experienced by the larvae, which can in turn influence the growth rate. The mean temperature experienced by all the larval samples in each year was therefore used with the fitted model to predict the relative growth rate of a “model” larvae, and the contribution of the year and temperature effects (Figure 9a). The variability in the year effect is clearly stronger than that due to the temperature effect, suggesting that the year effect is the more important of the two.

Furthermore, there is a significant difference in the growth rate before and after the onset of the reduced recruitment that cannot be accounted for by temperature changes. Years prior to the onset (1998, 1999) appear to have a significantly higher year-factor than those after the onset (2003, 2004) (Figure 9b). One approach to assess the significance of this observation is to replace the four-level year factor with a two-level “period” (*i.e.* pre and post) factor: such a simplification does not significantly change the fit of the model (Likelihood ratio test based on ML fit: LR = 4.14, df=2, p=0.13), suggesting it is a valid simplification. The simplified “period” model shows a significant reduction from the pre to the post level (one-sided *t*-test of period coefficient based on REML fit: t=3.10, df=42, p=0.002), with the factor for the “post” period being 12% lower than the “pre” period (Figure 9c).

Discussion

In this study we have shown a significant reduction in the recent (*i.e*. within the 21 days prior to capture) growth rate of herring late-larvae in the North Sea from 1998/1999 to 2003/2004. This reduction in growth coincides with the reduction in larval survival rates, and therefore with the reduced recruitment experienced in this stock. However, interpretation of these results is not straightforward and requires careful consideration.

Firstly, the applicability of the statistical model and its coefficients has to be considered. The model developed here attempts to explain the observed otolith growth-rates in terms of a number of covariates (length, temperature, photoperiod, spawning component) that are thought to play a role in the growth. Other effects that cannot be readily quantified but that are thought to be interannually variable, such as the amount or quality of food available to the larvae or predation pressures, end up being grouped into the year effect. The year- and period-coefficients (Figure 7b and 7c) therefore represent the "residual variability", once the other processes have been taken into account. Here we have shown that these processes dominate over the temperature changes, and encapsulate a significant reduction in growth that cannot be explained by the other covariates (such as temperature: Figure 7a) that we have considered.

Secondly, our results are based on the surviving larvae: large numbers of larvae died before the survey takes place and are not sampled in this analysis. We make the (implicit) assumption that the sampled larvae are representative of the entire population of spawned larvae, yet by the very fact that they survived long enough to be sampled, may in fact be outliers themselves. Changes in the growth rates of these survivors may, or may not, reflect the hidden processes occurring at the population level.

Taking these caveats into account, we can consider the potential mechanisms that may lead to the reduction in the observed growth rate.

Changes in the food supply could give rise to the observed results. If we assume a reduction in the amount or quality of the food available for herring larvae after the onset of the reduced-recruitment regime, then we would expect, on average, there to be an increased risk of starvation (especially during the winter months). Elevated starvation mortality would lead to a reduction in the total number of survivors (i.e. recruitment) and those that survived would exhibit a reduced growth rate, consistent with observations.

Reduced growth rates can also increase mortality, even when starvation is not important. Larval mortality is generally recognised as being length-dependent (big-is-better hypothesis (Leggett and DeBlois, 1997; Houde, 2002)), with increasing mortality rates at smaller sizes. Reductions in

growth-rate can therefore give rise to an increased amount of time being spent in a length-class, and therefore a greater exposure to predators (stage duration hypothesis, Houde, 2002)). The predation mortality rate could therefore increase with a reduction in growth rate, leading to a reduction in recruitment and the survivors growing slower, also consistent with observations.

Direct changes in the predation pressure also need to be considered as an alternative mechanism. An increase in a predator population or an influx of new predatory species could easily increase the predation pressure on the larvae and reduce the numbers of larvae that survive. However, without invoking a reduction in suitable prey for the larvae this would suggest a size selective mortality on the faster growing individuals.

In this simple analysis, changes in the food supply therefore appear to be a likely candidate mechanism. However, the simplicity of this reasoning may not reflect the complex reality of life in the ocean, and many other processes can be envisaged. Predation in particular is almost certainly not as simple as it is characterised here, and complex interactions can readily arise from the temporal and spatial overlap between species and the prey size-suitability interaction. Nevertheless, these mechanisms are useful for generating hypotheses and can readily form the basis for future investigations.

Otolith microstructure analyses are often predicated on the assumption that one otolith-ring corresponds to one day of growth, in spite of ample evidence that this assumption may not hold all of the time (e.g. Geffen 1982, Fox 2004). However, the approach employed here is expected to be robust to this weakness, as the analysis does not hinge upon this assumption. The approach used combines two different sources of data: otolith microstructure measurements, where we estimate the average growth rate over a period of 21 rings prior to capture and the hydrographic backtracking work, which averages the temperature and photoperiod over a period of 21 days prior to capture. In both cases we are using averaged, rather than integrated, quantities. Deviations from the one-ring-per-day assumption will therefore have a relatively minor impact on their value, and on the rest of the analysis.

The conclusions drawn here are naturally limited by the nature of the larval samples analysed. We have only considered two years before and after the onset of reduced-recruitment regime: adding other years will improve the analysis. Furthermore, our results are strongly biased towards larvae from the Buchan and Banks components that were captured in the central North Sea. Our analysis did not detect any significant difference between the spawning components, but it is also possible that we do not have enough samples to detect such a difference. Similarly, we have only considered larvae from the central North Sea: other regions almost certainly display different growth environments and dynamics. Interactions between factors were also not considered, due to the limited coverage of the data. Expansion of both the temporal and spatial

coverage of the larval samples is therefore necessary to increase both the generality and the statistical power of this result.

Conclusion

The results gathered here give a unique insight into the processes influencing the survival of larval herring. The initial hypothesis, that the reduction in larval survival during the reduced recruitment regime is associated with a reduction in growth rate, has been confirmed. The results, however, are limited to the four years considered, to the Buchan and Banks components in the first instance, and to larvae in the central North Sea. The exact mechanism via which the reduced growth-rate causes a reduction in larval survival also remains unclear, although changes in the food supply are a likely candidate. However, this work also introduces a unique and new observation that any hypothesis needs to both incorporate and explain. This work therefore represents a significant waypoint on the path to elucidating the mechanism underlying this challenging and enigmatic puzzle.

Acknowledgements

The authors wish to recognize the crews, captains, and scientists who have taken part in the International Bottom Trawl Survey over the past 30 years and have been instrumental in collecting the source material used in this study. The authors also wish to thank Morten Skogen of the Institute of Marine Research (IMR), Bergen, Norway, for providing the NORWECOM flow fields, and Audrey Geffen, University of Bergen, Norway, for inspiring conversations and constructive criticism. This study was funded in part by the project Defineit under the MariFish ERA-NET (ERAC-CT- 2006-025989), and by the IMR North Sea program.

References

AKSNES, D.L., ULVESTAD, K.B., BALINO, B.M., BERNTSEN, J., EGGE, J.K., SVENDSEN, E., n.d. ECOLOGICAL MODELLING IN COASTAL WATERS: TOWARDS PREDICTIVE PHYSICAL-CHEMICAL-BIOLOGICAL SIMULATION MODELS. Ophelia 41, 5-36.

Anderson, J.T., 1988. A review of size dependent survival during pre-recruit stages of fishes in relation to recruitment. Journal Of Northwest Atlantic Fishery Science 8, 55-66.

Batchelder, H.P., 2006. Forward-in-Time-/Backward-in-Time-Trajectory (FITT/BITT) Modeling of Particles and Organisms in the Coastal Ocean*. Journal of Atmospheric and Oceanic Technology 23, 727-741.

Borelli, G., Guibbolini, M.E., Mayer-Gostan, N., Priouzeau, F., de Pontual, H., Allemand,

Brophy, D., King, P.A., 2007. Larval otolith growth histories show evidence of stock structure in Northeast Atlantic blue whiting (Micromesistius poutassou). ICES Journal of Marine Science: Journal du Conseil 64, 1136.

Campana, Steven E. (2004): Photographic Atlas of Fish Otoliths of the Northwest Atlantic Ocean. Canadian Special Publication of Fisheries and Aquatic Sciences 133.

Christensen, A., Daewel, U., Jensen, H., Mosegaard, H., St John, M., Schrum, C., 2007. Hydrodynamic backtracking of fish larvae by individual-based modelling. Marine Ecology Progress Series 347, 221-232.

Clausen, Lotte Worsøe; Bekkevold, Dorte; Hatfield, E.M.C.; Mosegaard, Henrik (2007): Application and validation of otolith microstructure as a stock identification method in mixed Atlantic herring (*Clupea harengus* L) stocks in the North Sea and western Baltic. ICES Journal of Marine Science, 64(2), 377-385, doi:10.1093/icesjms/fsl036.

Cushing, D., Bridger, J., 1966. The stock of herring in the North Sea, and changes due to fishing.

Dickey-Collas, M., Nash, R.D.M., Brunel, T., van Damme, C.J.G., Marshall, C.T., Payne, M.R., Corten, A., Geffen, A.J., Peck, M.A., Hatfield, E.M.C., Hintzen, N.T., Enberg, K., Kell, L.T., Simmonds, E.J., 2010. Lessons learned from stock collapse and recovery of North Sea herring: a review. ICES Journal of Marine Science 67, 1875-1886.

Edwards, M., Johns, D., Licandro, P., John, A., Stevens, D., 2007. Ecological Status Report: results from the CPR survey 2005/2006, Ocean Science.

Fässler, S.M.M., Payne, M.R., Brunel, T., Dickey-Collas, M., 2011. Does larval mortality influence population dynamics? An analysis of North Sea herring (Clupus harengus) time series. Fisheries Oceanography no-no.

Feet PØ, Ugland KI and Moksness E. 2002. Accuracy of age estimates in spring spawning herring (*Clupea harengus* L.) reared under different prey densities. Fisheries Research, 56: 59-67.

Figueiredo, G.M. de, Nash, R.D.M. & Montagnes, D.J.S. 2005. The role of the generally unrecognised microprey source as food for larval fish in the Irish Sea. *Marine Biology* **148**: 395-404.

Folkvord A, Blom G, Johannessen A and Moksness E. 2000. Growth-dependent age estimation in herring (*Clupea harengus* L.) larvae. Fisheries Research, 46: 91-103

Folkvord A, Johannessen A and Moksness E. 2004. Temperature-dependent otolith growth in Norwegian spring-spawning herring (*Clupea harengus* L.) larvae. Sarsia, 89 (5) 297-310

Fox CJ, Folkvord A. and Geffen A.J. 2004. Otolith micro-increment formation in herring *Clupea harengus* larvae in relation to growth rate. Marine Ecology Progress Series, 264: 83-94

Gauldie, R.W., Nelson, D.G.A., 1990. Otolith growth in fishes. Comp. Biochem. Physiol. A97, 119–135.

Geffen AJ. 1982. Otolith ring deposition in relation to growth rate in herring (*Clupea harengus*) and turbot (*Scophthalmus maximus*) larvae. Marine Biology, 71: 317-326

Gröger, J. P., Kruse, G. H., and Rohlf, N. 2010. Slave to the rhythm: how large-scale climate cycles trigger herring (*Clupea harengus*) regeneration in the North Sea. ICES Journal of Marine Science, 67: 454–465.

Heath, M., 1993. An evaluation and review of the ICES herring larval surveys in the North Sea and adjacent waters. Bulletin of Marine Science 53, 795–817.

Heath, M., Henderson, E., Baird, D., 1988. Vertical distribution of herring larvae in relation to physical mixing and illumination. Marine Ecology Progress Series 47, 211-228.

Hjort, J., 1914. Fluctuations in the great fisheries of Northern Europe viewed in light of biological research. Rapports et Procés-Verbaux des Réunions de Conseil International pour l'Exploration de la Mer 20, 1–228.

Houde, E.D., 2002. Mortality. Chapter 3. pp. 64-87 In: L.A. Fuiman and R.G. Werner (eds). Fishery Science. The unique contributions of early life stages. Blackwell Science.

Hufnagl, M., Peck, M. a., 2011. Physiological individual-based modelling of larval Atlantic herring (Clupea harengus) foraging and growth: insights on climate-driven life-history scheduling. ICES Journal of Marine Science 68, 1170-1188.

Høie H, Folkvord A and Johannessen A. 1999. Maternal, paternal and temperature effects on otolith size of young herring (*Clupea harengus* L.) larvae. Journal of Experimental Marine Biology and Ecology, 234: 167-184

ICES, 2006. Report of the Planning Group of Herring Surveys (PGHERS), 24-27 January 2006 (No. ICES Document CM 2006/LRC:04). Rostock, Germany.

ICES, 2012. Report of the Herring Assessment Working Group of the Area South of 62 deg N (HAWG).

Johannessen A, Blom G and Folkvord A. 2000. Differences in growth between spring and autumn spawned herring (*Clupea harengus* L.) larvae. Sarsia, 85: 461-466.

Leggett, W.C., Deblois, E., 1994. Recruitment in marine fishes - Is it regulated by starvation and predation in the egg and larval stages. Neth. J. Sea Res. 32(2), 119-134.

McGurk MD. 1984. Ring deposition in the otoliths of larval pacific herring, *Clupea harengus* pallasi. Fishery Bulletin, 82: 113-120

McQuinn, I.H. 1997. Metapopulations and the Atlantic herring. Reviews in Fish Biology and Fisheries 7: 297-329.

Moksness E and Wepestad V. 1989. Ageing and back-calculating growth rates of Pacific herring, *Clupea pallasii*, larvae by reading daily otolith increments. Fishery Bulletin, 87: 509-513

Moksness E and Fossum P. 1991. Distinguishing spring- and autumn-spawned larvae (*Clupea harengus* L.) by otolith microstructure. ICES Journal of Marine Science, 48: 66-61

Moksness E. 1992. Validation of daily increments in the otolith microstructure of Norwegian spring-spawning herring (*Clupea harengus* L). ICES Journal of Marine Science, 49: 231-235

Montgomery, D.C., Peck, E.A., Vining, G.G., 2001. Introduction to Linear Regression Analysis, Technometrics. John Wiley & Sons.

Morales-Nin, B., 2000. Review of the growth regulation processes of otolith daily increment formation. Fish. Res. 46, 53–67.

Munk, P., Heath, M., Skaarup, B., 1991. Regional and seasonal differences in growth of larval North Sea herring (Clupea harengus L.) estimated by otolith microstructure analysis. Continental Shelf Research 11, 641-654.

Nash, R.D.M., Dickey-Collas, M., 2005. The influence of life history dynamics and environment on the determination of year class strength in North Sea herring (Clupea harengus L.). Fisheries Oceanography 14, 279-291.

Payne, M.R., 2010. Mind the gaps: a state-space model for analysing the dynamics of North Sea herring spawning components. ICES Journal of Marine Science 67, 1939-1947.

Payne, M.R., Hatfield, E.M.C., Dickey-Collas, M., Falkenhaug, T., Gallego, A., Groger, J., Licandro, P., Llope, M., Munk, P., Rockmann, C., Schmidt, J.O., Nash, R.D.M., 2008. Recruitment in a changing environment: the 2000s North Sea herring recruitment failure. ICES Journal of Marine Science 66, 272-277.

Pinheiro, J.C., Bates, D.M., 2000. Mixed-effects models in S and S-PLUS. Springer Verlag.

Puverel, D., Tambutte, S., Payan, E.P. 2003. Daily variations of endolymph composition: relationship with the otolith calcification process in trout. J. Exp. Biol. 206, 2685–2692.

SKOGEN, M.D., SVENDSEN, E., BERNTSEN, J., AKSNES, D., ULVESTAD, K.B., 1995. MODELING THE PRIMARY PRODUCTION IN THE NORTH-SEA USING A COUPLED 3-DIMENSIONAL PHYSICAL-CHEMICAL-BIOLOGICAL OCEAN MODEL. ESTUARINE COASTAL AND SHELF SCIENCE 41, 545-565.

Sinclair, M., 2009. Herring and ICES: a historical sketch of a few ideas and their linkages. ICES Journal of Marine Science 66, 1652-1661.

Skogen, M.D., Søiland, H., 1998. A Users Guide to NORWECOM 2.0: The Norwegian Ecological Model System. Fisken og Havet 18, 1-42.

Söllner, C., Burghammer, M., Busch-Nentwich, E., Berger, J., Schwarz, H., Riekel, C., Nicolson, T., 2003. Control of crystal size and lattice formation by starmaker in otolith biomineralization. Science 302, 282–286.

Thygesen, U., 2011. How to reverse time in stochastic particle tracking models. Journal of Marine Systems.

Vignon, M. 2012: Ontogenetic trajectories of otolith shape during shift in habitat use: Interaction between otolith growth and environment. Journal of Experimental Marine Biology and Ecology 420–421 (2012) 26–32

Wood, S.N., 2006. Generalized additive models: an introduction with R. CRC Press.

Zuur, A., Ieno, E., Walker, N., Saveliev, A., 2009. Mixed effects models and extensions in ecology with R.

Zuur, A.F., Ieno, E.N., Elphick, C.S., 2010. A protocol for data exploration to avoid common statistical problems. Methods in Ecology and Evolution 1, 3-14.

Vignon, M. 2012: Ontogenetic trajectories of otolith shape during shift in habitat use: Interaction between otolith growth and environment. Journal of Experimental Marine Biology and Ecology 420–421 (2012) 26–32

Zuur, A.F., Ieno, E.N., Smith, G.M., 2007. Analysing Ecological Data, Methods. Springer.

Tables

Table 1. Final model parameters

Effect	*Estimate*	*Std. Error*	*P value*
Length	0.0197089	0.00377878	0.0000
Temperature	-0.0971058	0.03456779	0.0076
yr1998	0.6126501	0.03674873	0.0000
yr1999	0.5844486	0.03405167	0.0000
yr2003	0.4433404	0.03556318	0.0000
yr2004	0.5329232	0.03797952	0.0000

Figures

Figure 1

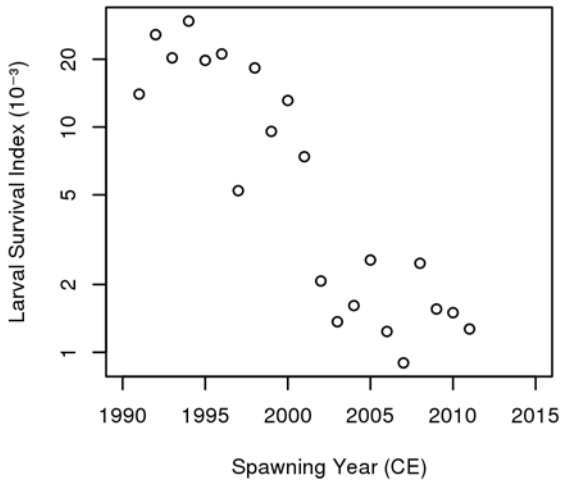

Figure 1 Time series of larval survival index (Nash and Dickey-Collas, 2005; Payne et al., 2008), defined as the ratio of the abundance of late-larvae (typically 20-30mm, as represented by the IBTS0 index (ICES, 2012)) to the abundance of early-larvae (less than 10-11mm, as represented by the SCAI index (Payne, 2010; ICES, 2012)). Survival ratio is plotted against the year in which the larvae are spawned. Note the logarithmic scale on the vertical axis. Adapted from (ICES, 2012).

Figure 2

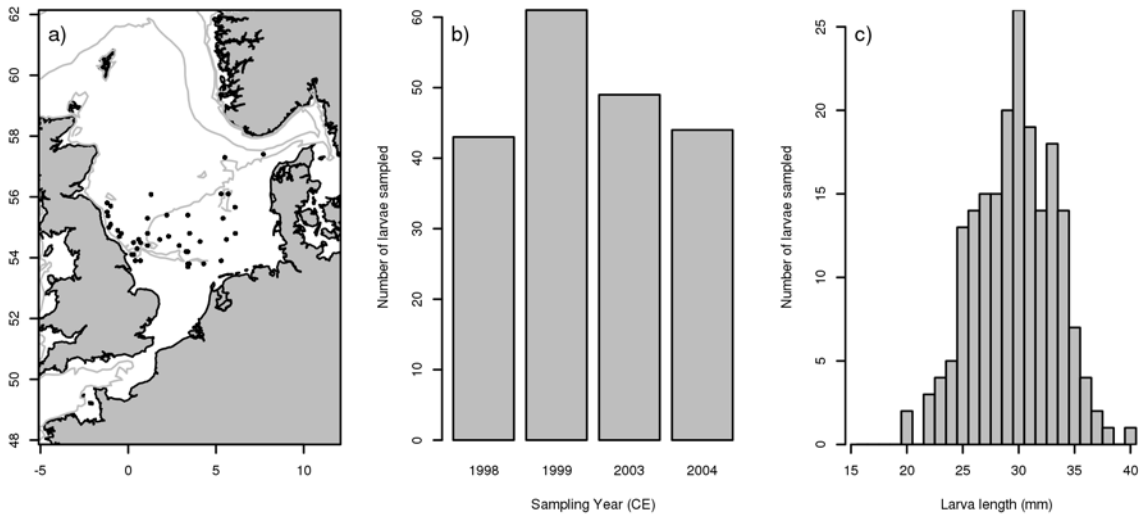

Figure 2. Distribution of larval samples a) Spatial distribution of samples across all years b) Distribution of samples taken between the four sampling years. c) Distribution of samples across larval lengths

Figure 3

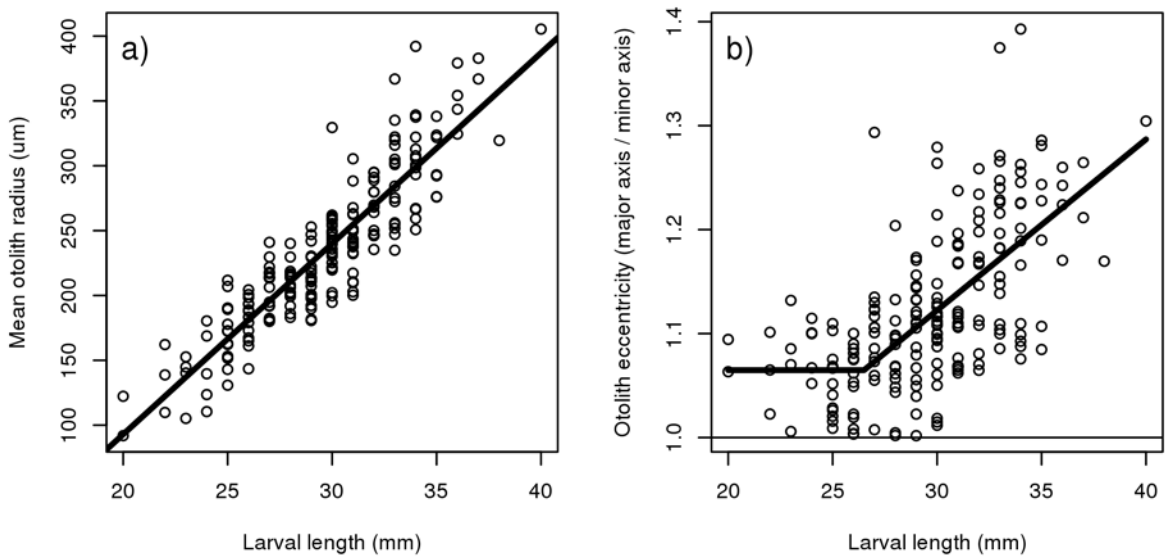

Figure 3. Relationship between otolith size and shape and larval size. a) Mean otolith radius as a function of measured larval length (round points), with fitted linear regression (heavy line). b) Changes in otolith shape can be visualised by plotting the eccentricity of the otolith (size of major-axis divided by the size of the minor-axis) against the size of the larvae. Line shows a break-point regression fit to the data, with the optimal break point at around 26.5mm.

Figure 4

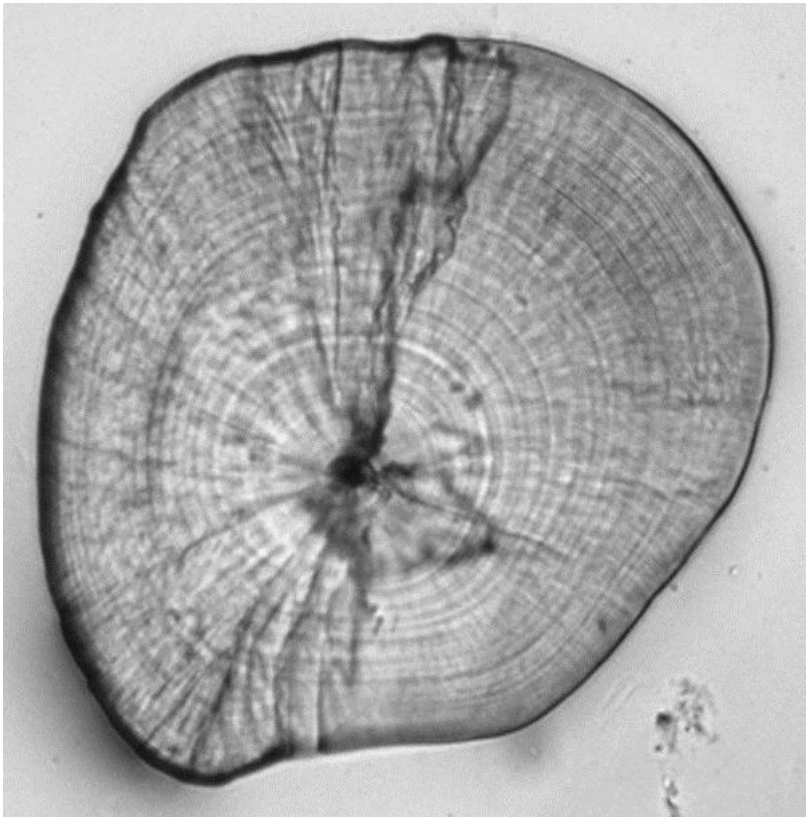

Figure 4. Picture of otolith from 30mm herring larvae (taken through a Leica microscope at 10x magnification).

Figure 5

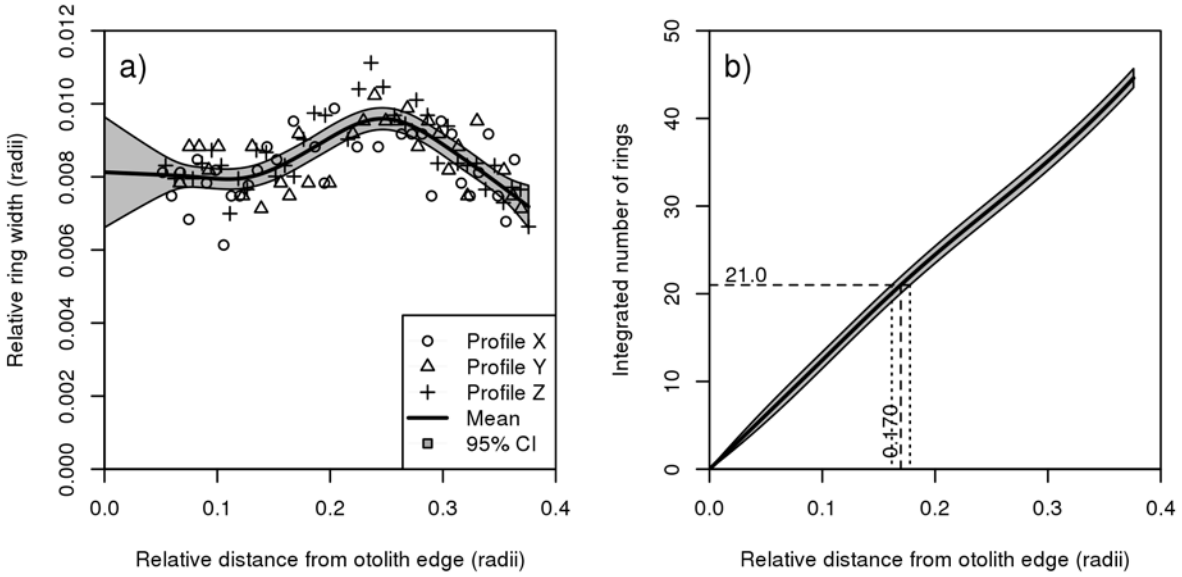

Figure 5. Estimation of otolith growth for picture shown in Figure 4. a). Relative ring widths (normalised by the radius of the otolith in the corresponding direction) are plotted as a function of the relative distance from the edge of the otolith (normalised in the same manner). The mean relative ring-width is estimated using a spline curve (heavy black link) and is shown together with the associated 95% confidence intervals (grey area). b) Integrated number of rings as a function of relative distance from the otolith edge (black line: mean, grey area: 95% confidence interval). The relative growth over a given period (in this example 21 rings) and associated confidence interval is estimated by reading off the corresponding value from the horizontal axis (in this case 0.170 radii).

Figure 6

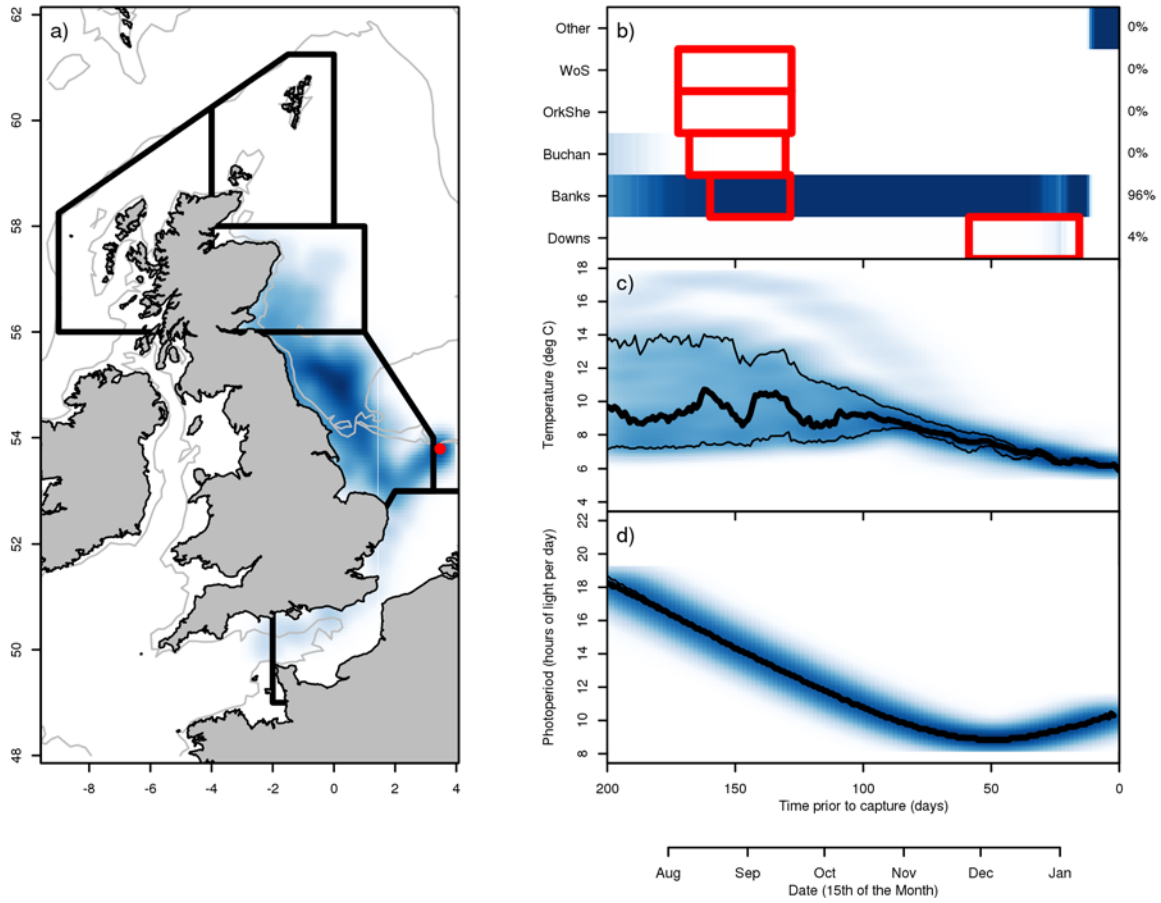

Figure 6. Reconstruction of environmental history for the larva shown in Figure 4 using hydrographic backtracking. a) Trajectory density of back-tracked particles released from the position of capture. Dark blue areas show the density of particles running backwards in time from the position where the larva was captured (red dot): darker colours indicate a higher density. The 50m and 200m isobaths are shown for reference (light grey lines). Heavy black lines denote the spatial regions associated with each spawning component. The components, clockwise from topleft, are: West of Scotland (WoS), Orkney-Shetland (OrkShe), Buchan, Banks and Downs. b) Assignment of larvae to a spawning component. The proportion of particles at a given time (horizontal axis) in each spawning region (vertical axis, following the abbreviations in a) is indicated by the colouring of each pixel – darker colours indicate higher proportions. The known spawning periods of each component are indicated by the red boxes. The estimated contribution of each component to the haul is indicated at right – this larva is clearly of "Banks" origin. c). Temperature history of the larvae, showing the density distribution of temperatures experienced by particles as a function of time. The median value (heavy black line) and central 95% confidence region (lighter black lines) are also shown. d) Photoperiod (daylight hours per day) experienced by the larva as a function of time prior to capture. Note that figures b, c, and d share a common time axis (number of days prior to capture) that is arranged so that time increases from left to right; the actual date is provided for reference.

Figure 7

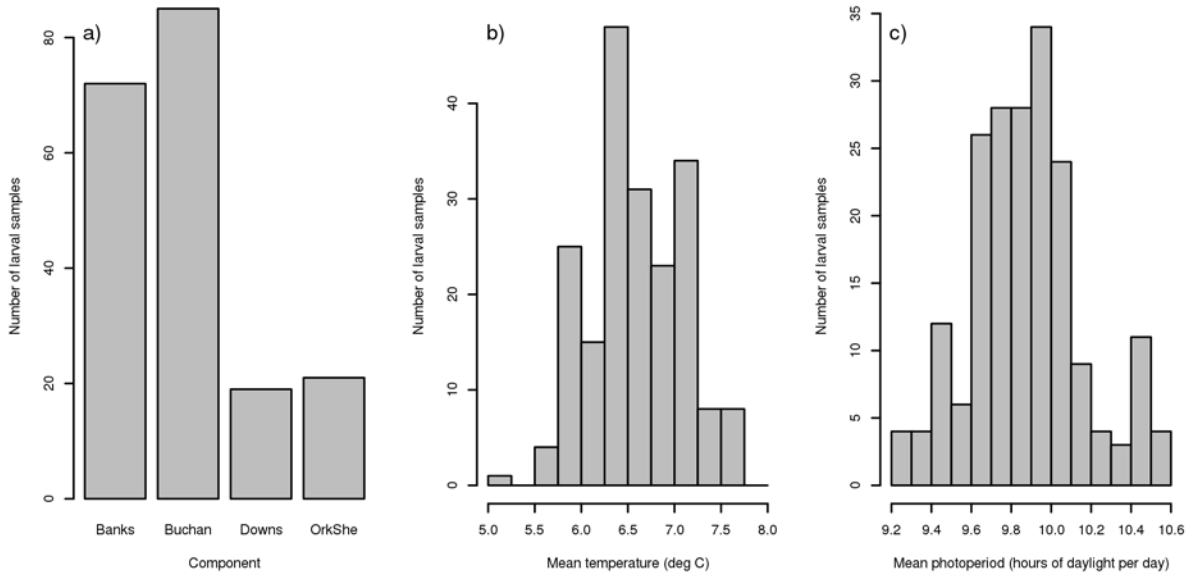

Figure 7. Summary of the backtracking results for all sampled larvae a) Number of larvae assigned to each of the spawning components: no larvae were assigned to the West of Scotland component. b) Distribution of estimated mean temperatures for given larvae during the 21 days prior to capture c) Distribution of mean photoperiods (hours of daylight per day) estimated for given larvae during the 21 days prior to capture as estimated from backtracking.

Figure 8

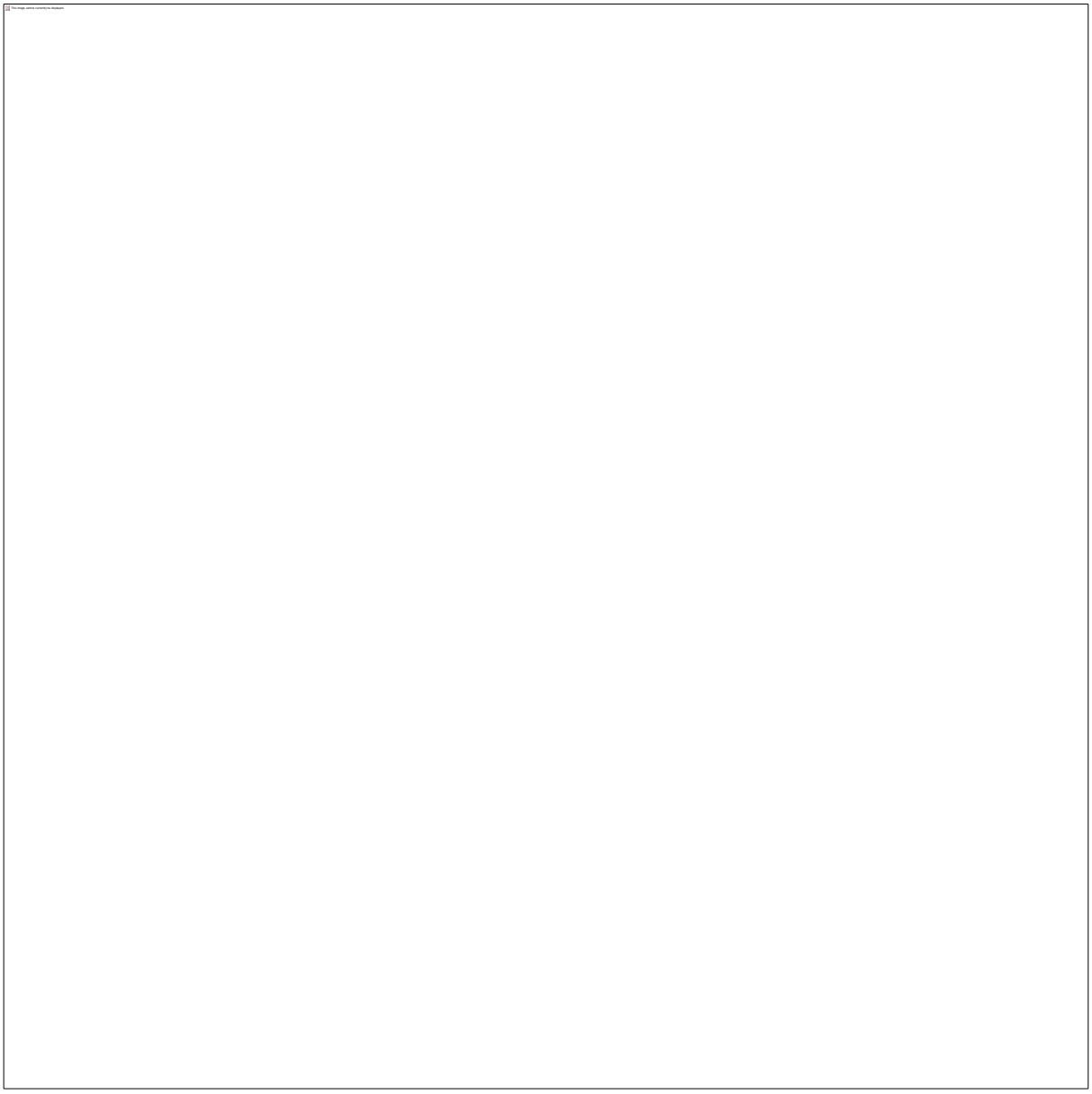

Figure 8 Mixed-effects model diagnostics a) Tukey-anscombe plot, plotting the Pearson (standardised) residuals from the model against the fitted value of the otolith growth rate. Note that the growth rate is fitted as the log-transformed value, and is therefore plotted on a logarithmic scale. b) Pearson residuals plotted as a function of larvae length dc Pearson residuals plotted as a function of the mean temperature. d) QQ plot, plotting the Pearson residuals against the corresponding quantiles of a standard normal distribution (dots). The 1:1 line is drawn for reference.

Figure 9

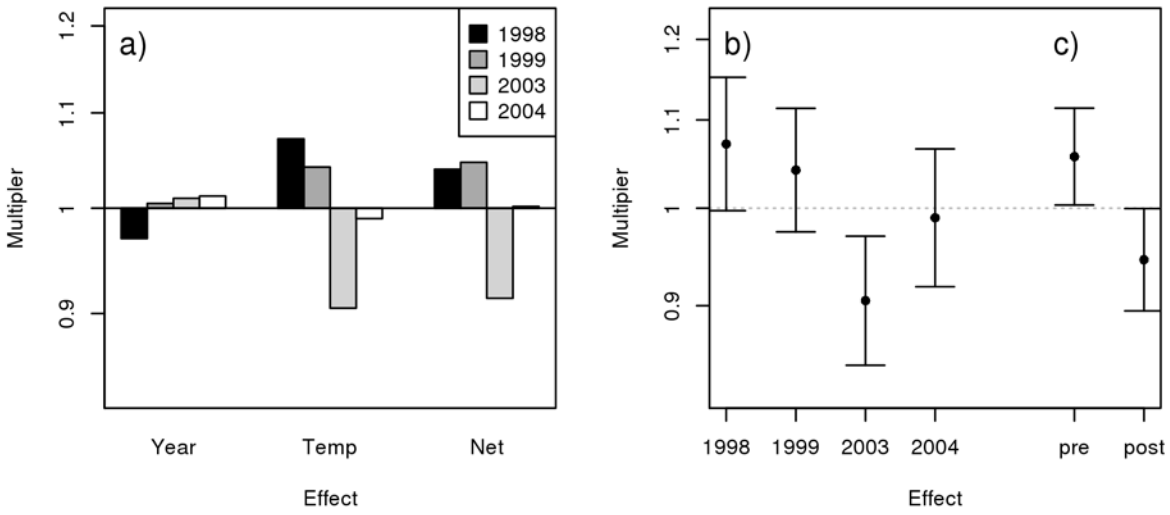

Figure 9. Fitted model coefficients a) Individual contributions of the year effect, temperature and net effect for the individual years. The temperature and year effects are calculated using the average values, whilst the net effect is the product of the two *i.e.* Net multiplier = Temperature multiplier * Year multiplier b) Year coefficients from the fitted model, with 95% confidence intervals c) Coefficients from the "period" model, where time is expressed as a pre- and post-2000 factor, with 95% confidence intervals. Note that in both panels the model coefficients are expressed as relative multipliers *i.e.* the multiplicative effect that they have on the growth rate, relative to the mean effect. Note also the logarithmic scaling of the vertical axis of both panels.